Fiber-fed Pulsed Plasma Thruster (FPPT) with Multi-axis Thrust Vectoring

IEPC 2022-558

Presented at the 37th International Electric Propulsion Conference
Massachusetts Institute of Technology, Cambridge, MA USA
June 19-23, 2022

Curtis A. Woodruff[1], Magdalena Parta[2], Darren M. King[3], Rodney L. Burton[4], and David L. Carroll[5]
CU Aerospace (CUA), Champaign, IL 61822, USA

Abstract: CU Aerospace (CUA) has developed the coaxial Fiber-fed Pulsed Plasma Thruster (FPPT) with multi-axis thrust vectoring capability that can enable high impulse primary propulsion missions for small satellites. Thruster subsystem testing of a 1.7U system configuration with a 26 J energy storage unit (ESU) operating at 78 Watts (3 Hz) produced a mean thrust of 0.60 mN with a specific impulse of 3,500 s and an efficiency of 13%. Thruster performance varies with fuel feed rate. Accelerated subsystem life testing demonstrated > 1.6 billion capacitor charge / discharge cycles with nearly identical current waveforms. The capability for independent control of input power and propellant feed rate allows tuning both thrust level and Isp. Testing to date shows electromagnetic thrust vectoring capabilities on the order of ±10 degrees in the pitch and yaw axes. Furthermore, the system has the potential to provide control authority on the roll axis. The pitch and yaw thrust vectoring performance are presented alongside recent thruster performance improvements. A 1.7U FPPT with 28,000 N-s of total impulse is being integrated for flight on CUA's NASA-funded Dual Propulsion Experiment (DUPLEX) CubeSat, presently manifested for launch in Q1 2023. FPPT technology is a compelling option to meet many micropropulsion needs including extended orbital maneuvers, collision avoidance maneuvers, deep-space missions, drag makeup, and deorbiting.

Nomenclature

B = *azimuthal magnetic field, T*
B_z = *axial magnetic field, T*
b = *constant in thrust equation, non-dimensional*
dt = *differential time step, s*
E = *electric field, V/m*
e = *electron or ion charge, 1.6 x 10 $^{-19}$ coulombs*
f = *thruster pulse rate, Hz*
g = *gravitational acceleration, 9.81 m/s^2*
I = *pulse current, amperes*
I_{bit} = *impulse bit = $\int I dt$, N-s*
I_{sp} = *specific impulse U_e/g, seconds*
J = *energy, joules*
j = *current density, amperes/m^2*
$\boldsymbol{jxB}$ = *electromagnetic force density, N/m^3*
L' = *inductance gradient, H/m*
m = *ablated propellant mass per pulse, kg*
m_e = *mass of electron, kg*
PCB = *Printed Circuit Board*
PPU = *Power Processing Unit*
PPT = *Pulsed Plasma Thruster*
$PTFE$ = *polytetrafluoroethylene $(C_2F_4)_n$ [Teflon]*
r_i = *radius of inner electrode (anode), m*
r_o = *radius of outer electrode (cathode), m*
R_{oi} = *radius ratio r_o/r_i of outer and inner electrodes*
s/c = *spacecraft*
T = *mean thrust = $f\ I_{bit}$, N*
U_c = *Alfven critical speed, km/s*
U_e = *propellant mean exhaust velocity = I_{bit}/m, m/s*
ΔV = *$g\ I_{sp}\ ln(m_o/m_f)$, m/s*
η_{PPU} = *PPU efficiency, power output / input*
Ψ = *action integral $\int I^2 dt$, A^2-s*

[1] Senior Engineer, woodruff@cuaerospace.com.
[2] Staff Engineer, magda@cuaerospace.com.
[3] Laboratory Director, king@cuaerospace.com.
[4] VP for Research, burton@cuaerospace.com.
[5] President, carroll@cuaerospace.com.

I. Introduction

The pulsed plasma thruster (PPT) [Burton, 1998] has long been an attractive technology for satellite propulsion. The PPT uses solid propellant and therefore inherently eliminates the possibility of propellant leakage and undesirable leakage thrust or contamination. The first electromagnetic PPT flight was on the Soviet Zond II Mars mission in 1964 [Burton, 1998]. One of the first published papers on the PPT was in 1965 [Guman, 1965]. After Zond II, important PPT flights occurred in 1981 (TIP/Nova) [Ebert, 1989; Hoffman, 1992], 1968 (LES-6) [Guman, 1970] and 2000 (EO-1) [Benson, 2000; Zakrzwski, 2002]. Despite this extensive flight history, fundamental improvements still remain to be made in PPT propulsion systems, and we present several such advances in this paper.

Propulsion systems for CubeSats are evolving with a wide variety of thrust, specific impulse, and power draw levels and corresponding trade-offs, but still very few have flown to date. A good summary of CubeSat propulsion systems through 2016 is provided by Lemmer [2017]. A relatively new option is the coaxial Fiber-fed Pulsed Plasma Thruster (FPPT) [Woodruff, 2019a-b; Burton, 2021] for small satellites which can enable high impulse, high specific impulse primary propulsion missions by the combination of a user-controlled Teflon fiber feed system employing a different propellant *jxB* topology from that of classic PPT configurations, a regenerative carbon igniter, and low mass ceramic capacitors. A major enhancement of the FPPT technology is the ability to control the propellant feed rate along with the pulse energy and pulse rate, thereby providing control of both specific impulse and thrust. Other advantages of the FPPT technology include: (i) no pressure vessel or microvalves are required thereby significantly reducing cost, (ii) solid inert Teflon propellant which brings simplicity, safety and a wide operating temperature range to the fuel feed system, (iii) spooled propellant storage inside the thruster package which is easily expanded as needed, (iv) packaging as small as 1U, and (v) a volume envelope well-suited for 6U or larger CubeSats. FPPT utilizes completely non-toxic solid propellant Teflon, has no corrosive or propellant plugging issues, and provides on-demand thrust with no pre-operation warmup time requirement. The geometry of FPPT enables a highly integrated electromagnetic vectoring system acting on the primary thruster plasma to change the direction of its exhaust velocity vector that is more compact, less expensive, and with lower mass than a mechanical gimbal system. Thrust vectoring/steering with the FPPT system has emerged as a highly desirable capability for the purposes of spacecraft attitude control and for desaturating attitude control reaction wheels, particularly for deep space missions where a spacecraft is beyond Earth's electromagnetic field such that magnetic torque rods or coils can no longer be used for wheel desaturation.

In this paper we describe the design and developmental testing of the technology in **Section 2**, experimental performance data and geometry optimization studies in **Section 3**, electromagnetic thrust vectoring in **Section 4**, and the 1.7U FPPT flight hardware for the Dual Propulsion Experiment (DUPLEX) CubeSat mission in **Section 5**.

II. Technology Description

2.1. General Design

A schematic of the FPPT system is shown in **Figure 1**. The thruster is evolved from earlier CUA FPPT designs [Woodruff, 2019a; Woodruff, 2019b; Burton, 2021] using a 3D printer fiber feed system, which pulls a Teflon fiber from a spool. Note that an anode feed stop lip is not used on FPPT as with classic PPTs, as the feed system provides a variable rate of feed, which in combination with the plasma pinch discharge self-forms a shaped (usually conical) end tip to the propellant [Woodruff, 2019b]. Unlike previous versions of FPPT, embedded electromagnets have been added to the back side of the thruster insulator to provide thrust vectoring capability, **Section 4**.

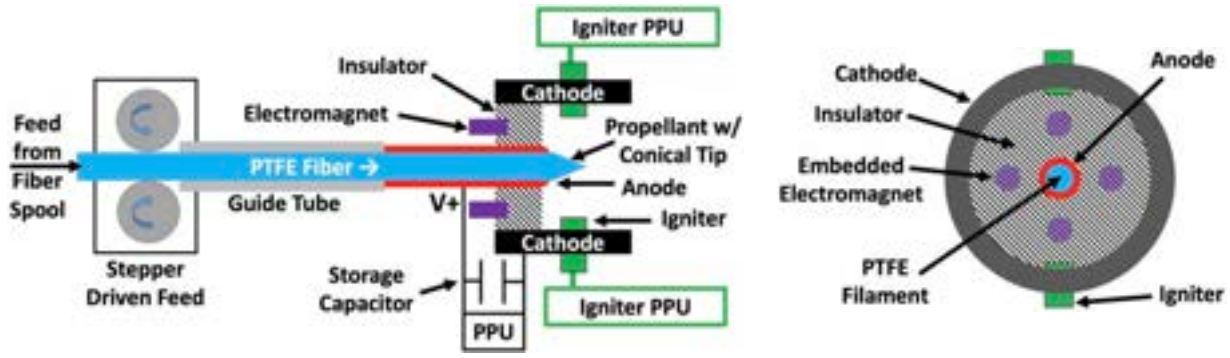

Figure 1. Cross-section (left) and end view (right) schematics of the FPPT with cylindrical cathode.

2.2. Propellant Storage Development and Feed Testing

The original 1U FPPT design planned to use a round spool similar to that used for CUA's Monofilament Vaporization Propulsion (MVP) system [Woodruff, 2018; Woodruff, 2022]. Early in the FPPT design process it was decided to increase the 1U geometry to a 1.7U configuration that would accommodate more capacitance and propellant. This increase in width from a 1U system to the 1.7U layout changed the spool layout from circular to a racetrack configuration. The shape was designed to allow for parallel stacking of propellant and retain self-similarity as the spool was wound. However, it was determined through testing that the flattened (racetrack rather than circular) spool geometry was incompatible with the unspooling technique previously used by the MVP circular spool system; unspooling from the outside of the racetrack configuration presented some technical issues that resulted in snagging during unwinding. This feed issue was resolved by pulling propellant from the interior of the coil, similar to a skein of yarn unspooling, rather than around the exterior of the spool as done with MVP.

A clear test spool apparatus was fabricated, **Figure 2**, where the propellant was wound from inside to outside around the semicircular posts which are bolted between the clear acrylic plates. Once the spool was fully wound, the standoffs around the spool perimeter were installed. Following this, the posts were unscrewed and removed through the large center holes. This system allows propellant to be wound into a flight "caddy" and never transferred out of its original winding enclosure, ensuring reliable unspooling without internal tangles. The test spool shown in **Figure 2** was completely unwound without tangling or snagging over multiple tests. With this system propellant loads in the proposed range of 800-900 grams are possible and can possibly be exceeded.

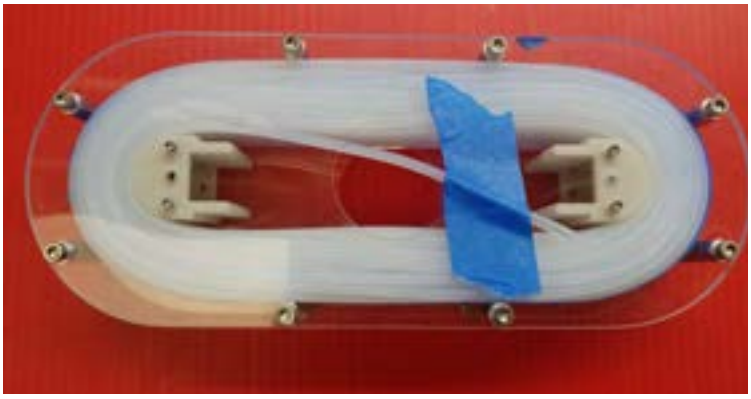

Figure 2. Internal unspooling test hardware.

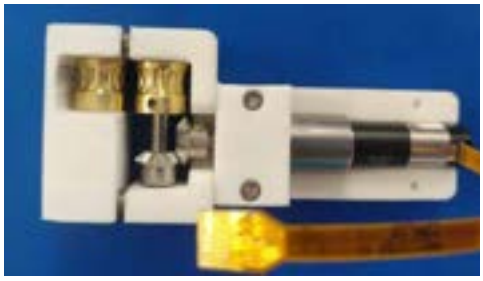

Figure 3. Assembled feed system.

A prototype of the motor drive system was produced and tested, **Figure 3.** Shims can be added between the roller pieces to adjust propellant squeeze. This system was successfully implemented and tested for repeatedly pulling the full loads of Teflon propellant filament.

2.3. Capacitor Bank Development and Testing

Capacitor Life Testing

A small scale, accelerated life test in atmosphere was initiated to test charge-discharge cycles with realistic loading, i.e., peak current for an individual capacitor during a typical FPPT firing of ~25 amps and pulse duration to the first reversal of ~6 microseconds. **Figure 4** shows the waveform of the accelerated test as compared to earlier data with a 15.2 J capacitor bank [Woodruff, 2019a]. Each current waveform is divided by the total capacitor count (6 for accelerated test apparatus, 656 for FPPT current traces). To achieve relatively similar waveforms between the accelerated test rig and a full-scale capacitor bank, a high current IGBT switches the small capacitor bank through a dummy load of 2 ohms and 2.8 μH. A diode allows for the current reversal. Note that the accelerated test uses a pulse with a higher current peak and dI/dt than anticipated with the flight unit, representing a more extreme stress test than the flight unit should experience.

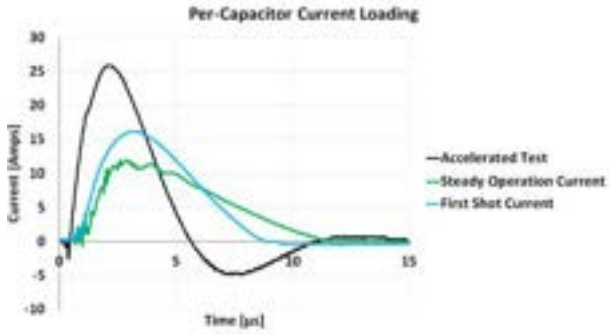

Figure 4. Waveform comparison between accelerated test setup and actual FPPT firings.

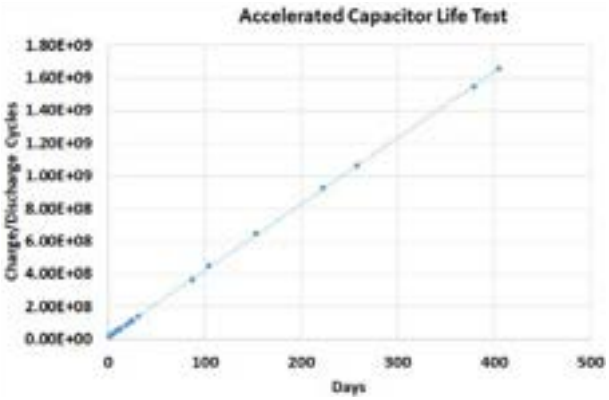

Figure 5. Number of charge/discharge cycles as function of time for continuous operation over > 400 days. (Points denote oscilloscope verification days.)

This setup was charged and discharged at a rate of ~ 50 Hz and operated 24/7 for over 400 days, accumulating 1.66 billion charge-discharge cycles without failure, **Figure 5** (note that the points denoted were days where the test was paused briefly to verify that the pulse waveform was essentially identical to prior days). No change was seen in the current traces throughout the experiment. Note that the 1.7U flight unit described in **Section 5** should only experience ~ 124 million pulses for its propellant load, so that the 50 Hz test result is equivalent to processing over 10 kg of propellant for an impulse of 370,000 N-s.

Capacitor Bank Testing

A 2.6 J capacitor bank module was fabricated and tested extensively for development and reliability, **Figure 6**. This bank has now been operated for over 221,000 pulses without failure. The 1.7U FPPT flight capacitor bank geometry design underwent multiple iterations and includes four (4) larger modules with ~ 8 J maximum energy storage per module that were assembled with this technique and placed in the final FPPT hardware assembly for a total of 32 J of energy storage capacity. The final version includes 1232 MLCC capacitors having ~31.5 J effective bank energy. The arrangement shown in **Figure 7** allows for a reduced part count for the double-layer bank.

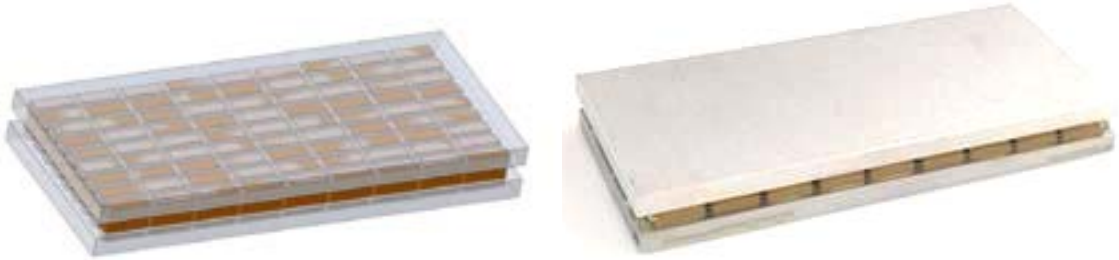

Figure 6. Assembled capacitor module CAD (left) and photo (right) with 81 MLCC capacitors and 2.6 J of energy storage capacity. To date, this assembly has survived 221,000 pulses without failure.

Figure 7. Flight capacitor bank with 1232 MLCC capacitors storing a total of ~31.5J of energy.

2.4. *Igniter Development and Testing*

The flight igniter circuit was developed on a small standalone circuit board to better facilitate testing and to allow for tuning and adjustments before the final boards are produced. The populated board is shown in **Figure 8**. **Table 3** shows the characteristics of the igniter circuit. The circuit was run for >150,000,000 pulses without failure.

Figure 8. Development igniter circuit.

Igniter erosion data is acquired when running thruster tests, and the shorter length cathodes (discussed in Section 3.2) has performed exceedingly well in this respect. An example test accumulated 32,000 shots, during which time the igniter averaged a mass gain of 0.03 µg per shot. This type of wear profile, i.e., a very gradual accumulation of carbon, prevents electrode wear and should be sustainable for full system life. Igniter location and recess is also critical in achieving a neutral erosion state and must be reconfirmed in the event of a configuration change. More information on and an image of the igniters can be found in [Woodruff, 2019].

Table 3. Igniter circuit parameters.

Igniter Pulse Circuit	Value	Unit
Total Capacitance	0.64	µF
Voltage	800	V
Total Energy	0.20	J
Time to Peak Current	1	µs
Time to Main Ignition	2	µs

2.5. *Overall Circuit Design and Grounding*

To minimize chances for electromagnetic interference (EMI) effects to the rest of the DUPLEX satellite, great care was taken to design the thruster circuitry and provide some shielding to contain the EMI pulses naturally generated in a PPT system. **Figure 9** shows a circuit diagram of the FPPT flight system designed with guidance from NASA GRC personnel to minimize EMI. A 1 MΩ resistor with a 2200 pF capacitor couples isolated HV ground to signal ground. Another 1 MΩ resistor on the PCB couples signal ground to the PCB enclosure. And the PCB enclosure is coupled to the chassis ground through seven aluminum screws fastened to the chassis frame.

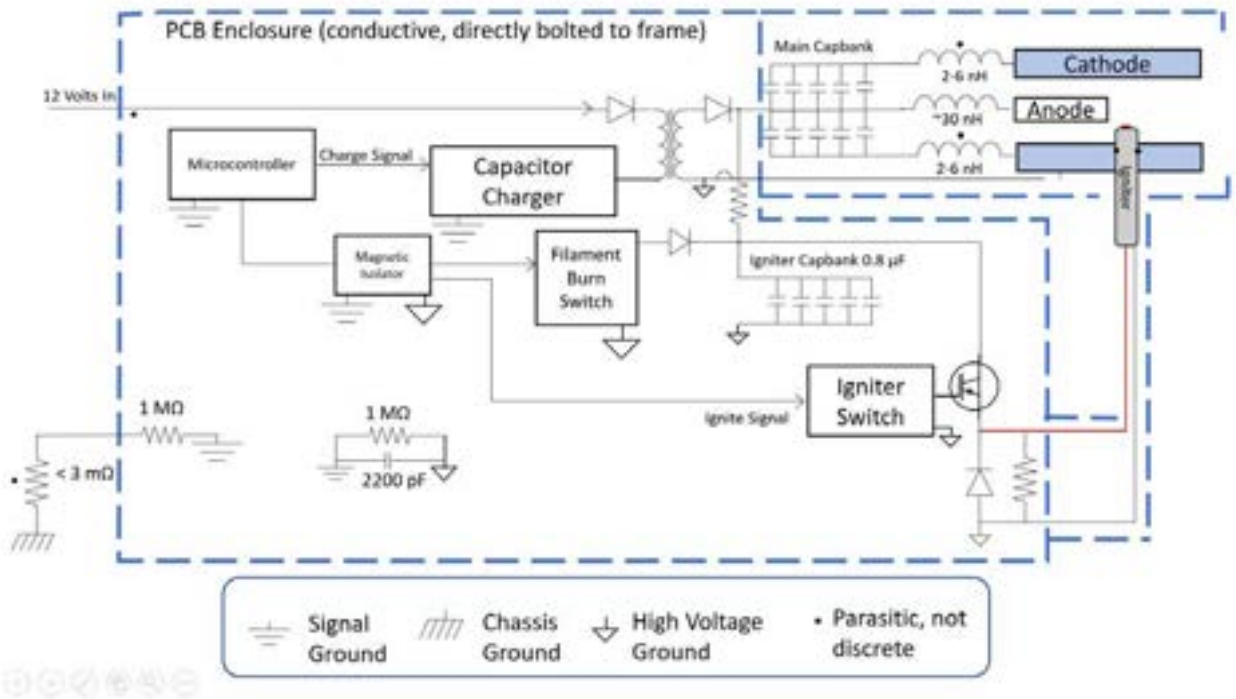

Figure 9. Circuit diagram of FPPT system showing grounding to minimize EMI.

III. Thrust Stand Performance Testing

3.1. Cathode and Anode Development and Testing

Multiple cathode and anode sizes were investigated to optimize the geometry and maximize performance. The electromagnetic contribution to thrust is predicted for coaxial geometries by:

$$T = (\mu_o/4\pi)\, I^2\, [ln(R_{oi}) + b] \tag{1}$$

where $1/4 < b < 3/4$ [Jahn, 1968] and R_{oi} is the radius ratio r_o/r_i of outer and inner electrodes. For current pulses, the integration over the current pulse of the thrust equation, assuming that the discharge geometry is invariant, results in an impulse bit proportional to the action integral $\Psi = \int I^2 dt$. Comparison of the predicted impulse bit to the total impulse bit measured on the thrust stand shows that the FPPT electromagnetic contribution to thrust is > 95% with the most recent configurations [Burton, 2020], with the remaining < 5% being electrothermal.

As with any coaxial electromagnetic thruster, it is tempting to increase the radius ratio of the outer electrode to the inner electrode, to increase $ln(R_{oi})$ and take advantage of the higher thrust and dynamic impedance $L'U_e/4$. From work with quasi-steady magnetoplasmadynamic (MPD) thrusters [Ekdahl, 1967; Burton, 1983] it is known that for sufficiently large R_{oi} the discharge can collapse from azimuthal symmetry into a radial spoke. While it is not known what the R_{oi} limit is for pulsed (not quasi-steady) PPTs, the FPPT originally used a conical cathode with an average $R_{oi} \approx 5$ and showed no evidence of spoking. However, for the 1.7U flight design, a cylindrical cathode is preferred for packaging reasons, with the electrode geometry shown in **Figure 1**. Photographs from four tested geometries (conical, 22.3 mm cylindrical,35.0 mm cylindrical, and 49.0 mm cylindrical) are shown in **Figure 10**; all three show similar characteristics including a central plasma pinch column discussed elsewhere [Woodruff, 2019b; Burton, 2021] and notably absent spoking.

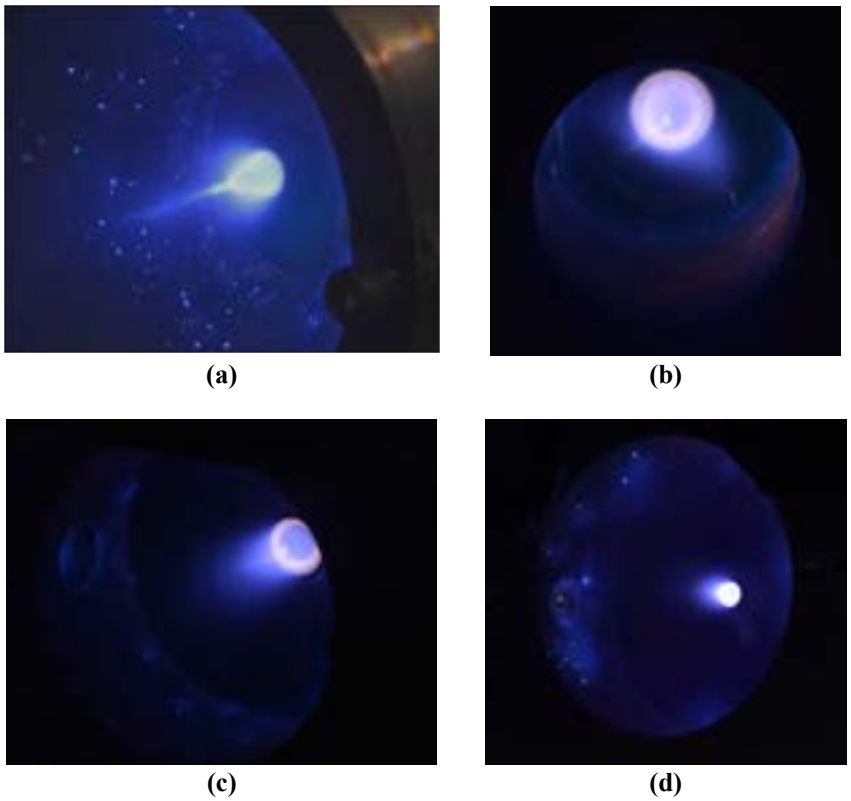

(a) **(b)** **(c)** **(d)**

Figure 10. Photographs of the Fiber-fed Pulsed Plasma Thruster (FPPT) during operation: (a) conical cathode with average diameter of ~35 mm; (b) 22.3 mm cylindrical cathode; (c) 35.0 mm cylindrical cathode; and (d) 49.0 mm cylindrical cathode. The discharge displays a central pinch column and cathode spots.

3.2. Thrust Stand Testing

Thrust stand measurements were made with the FPPT thruster subsystem to validate performance relative to prior testing [Woodruff, 2019a; Burton, 2021]. All data is taken on CUA's replica of a Watt's inverted pendulum compact thrust stand described in [Hejmanowski, 2015]. FPPT performance has been mapped across a variety of parameters – fuel feed, ESU capacitance, ESU energy, pulse rate, and total power. Incremental improvements through the development program have yielded a handful of targeted operating conditions [Woodruff, 2019a]. A unique trait of the FPPT system is that for a given input power, the thruster head has been demonstrated to operate stably over a range of fuel feed rates. This gives rise to a range of operating conditions with differing steady-state exposed fuel shapes and their associated performance points. Before taking the thrust measurement, each of the unique operating conditions shown was fired for a minimum of 10,000 pulses to ensure a properly formed propellant cone and an accurate I_{sp} calculation. Each measurement is an average of the turn-on and turn-off thrust level with a ±5% shot-to-shot repeatability.

Multiple cathode radius r_o and anode radius r_i configurations were tested with the general trend showing that higher r_o/r_i generates higher specific impulse and efficiency, **Table 4,** and **Figures 11 – 13**. The lowest performing efficiency case corresponded to the lowest r_o/r_i of 3.3 and when r_o/r_i reached 7.6 it was possible to achieve an efficiency of > 13% and specific impulse of 3500 s, **Figure 13**. The adjustment to anode outer diameter had a dramatic effect on the performance of the thruster by more than doubling the efficiency and increasing the I_{sp} to as high as 3600 s with the smaller diameter anode. While testing with Case 4 provided the highest performance, this case had an anode wall thickness of only ~ 0.5 mm and indicated that erosion would likely be an issue (not suitable for flight) with this smaller exposed anode area. Therefore, Case 5 was tested having a thicker anode wall and smaller propellant filament size resulting in no anode erosion of significance (as was also true for Cases 1 – 3). For the largest R_{oi} case of 10.7 having a 49 mm diameter cathode (Case 6), while the radius ratio increased, the measured Isp was lower which may be a consequence of an observed decrease in the current trace. Overall, the data indicate a peak in efficiency at a R_{oi} of 7.5 – 8.0. *The geometry of Case 5 was selected for the 1.7U FPPT flight unit for DUPLEX.*

Table 4. Experimental data for different discharge geometries (cathode inner diameter and anode outside diameter) having lower propellant feed rate and higher I_{sp}.

Parameter \\ Cathode Geometry	**Case 1 Conical**	**Case 2 Cylindrical**	**Case 3 Cylindrical**	**Case 4 Cylindrical**	**Case 5 Cylindrical**	**Case 6 Cylindrical**
Cathode Inner Diameter (mm)	35 mm	22.3 mm	35 mm	35 mm	35 mm	49 mm
Anode Outer Diameter (mm)	7.6 mm	6.8 mm	6.8 mm	4.4 mm	4.6 mm	4.6 mm
R_{oi} = Cathode ID / Anode OD (mm)	4.6	3.3	5.1	8.0	7.6	10.7
Anode Inner Diameter (mm)	3.3 mm	3.3 mm	3.3 mm	3.4 mm	2 mm	2 mm
Cathode Length (mm)	25.4 mm	19.1 mm	25.4 mm	16.5 mm	16.5 mm	23 mm
Bank Energy (J)	32	26	26	26	26	26
Mass per pulse (µg/pulse)	7.74	5.27	5.27	5.27	5.27	5.27
I_{bit} (µN-s)	182	132	124	186	183	150
I_{sp} (s)	2400	2550	2450	3600	3500	2800
Efficiency (%)	6.4	5.1	5.8	13.0	12.2	8.2
Peak Current (kA)	13.0	11.3	11.3	15.1	14.7	14.1
Thrust-to-Power, T/P (µN/W)	5.4	4.1	4.7	7.3	7.0	5.8
Notes		Lowest η		High Erosion	DUPLEX	

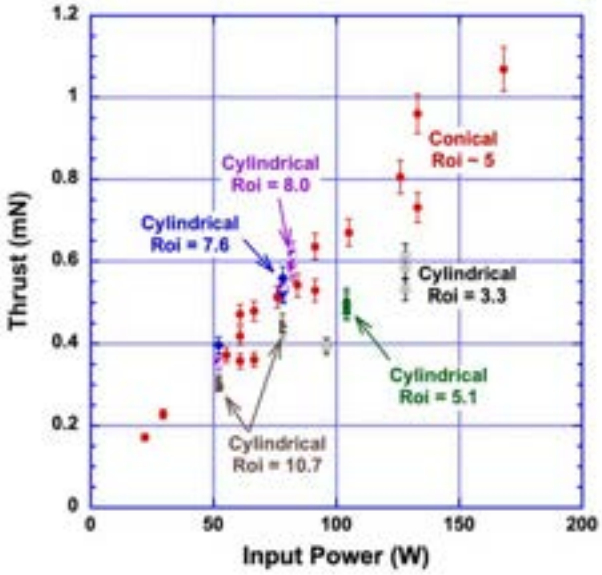

Figure 11. Total thrust versus input power as a function of the cathode-to-anode diameter ratio R_{oi}. (Shot-to-shot repeatability of ± 5%.)

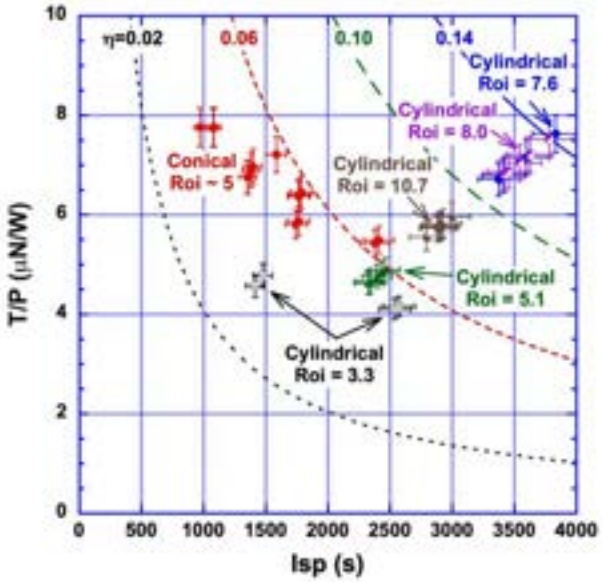

Figure 12. Specific thrust versus Isp as a function of the cathode-to-anode diameter ratio R_{oi} including constant efficiency lines. (Error bars are ± 5%.)

Figure 11 shows thrust versus input power for the different configurations; note that the more recent cylindrical cathode data were limited in pulse rate to 3-4 Hz by the capacitor charging circuit of the flight-like electronics that are to be implemented on the DUPLEX flight system.

Figure 12 shows specific thrust (μN/W) as a function of the specific impulse for different cathode-to-anode radius ratio configurations. The original FPPT goal of 1200 s was nearly tripled, with peak performance surpassing 3500 s. As mentioned earlier, data points were always preceded by over 10,000 firings to ensure an accurate feed rate (and mass flow) determination. For a given radius ratio R_{oi} the specific thrust $T/P = 2\eta/gI_{sp}$ tends to decrease with increasing I_{sp} (though more data would be required to better establish this for the cylindrical $R_{oi} = 5.1 – 10.7$ cases).

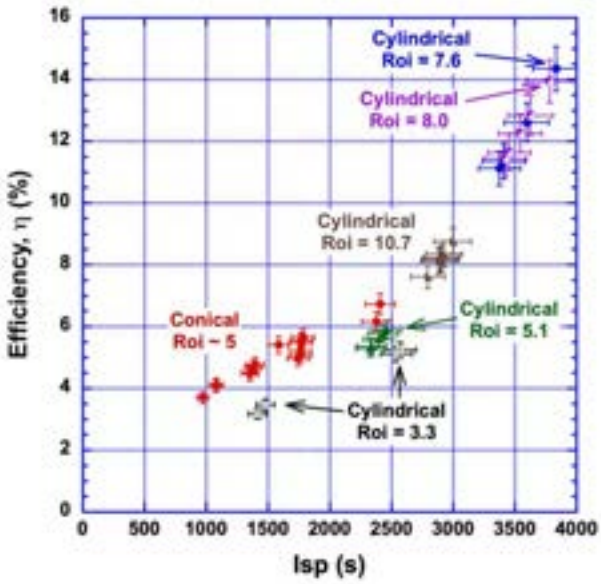

Figure 13. Thrust efficiency versus specific impulse as a function of the cathode-to-anode diameter ratio R_{oi}. (Error bars are ± 5%.)

Figure 13 shows thruster efficiency as a function of specific impulse and is found to increase approximately linearly with I_{sp}. The observed linear increase in efficiency is expected for a high-I_{sp} electromagnetic thruster with low electrothermal thrust, since the electromagnetic impedance $Z_{em} = ¼L'U_e$ is linear in I_{sp}, and the thruster efficiency

is $\eta_t = Z_{em}/(V_o/I)$. The ~ 3500 s conditions are the most electrically efficient cases at over 12%. Heritage PPT-11 data showed efficiencies exceeding 10% were possible [Laystrom, 2003], and a CUA NASA-funded SBIR Phase II FPPT development program in fact demonstrated efficiencies exceeding this 10% mark. Thruster efficiency is computed by dividing the thrust power ($T*U_e/2$) by supply power. The capacitor charging power supply input is monitored, and its rated efficiency is applied to the measured supply wall power draw when calculating the power into the thruster capacitors. To date, efficiency increases have been modest with higher discharge energy and more significant with higher I_{sp} (via feeding less propellant per Joule).

Anode erosion in FPPT is very low with values between immeasurable and ~0.20 μg/pulse depending on operating conditions. These erosion rates compare to fuel ablation rates of 5-10 μg / pulse for nominal 32 J operating conditions. Anode erosion was minimized with lower fuel feed conditions corresponding to high I_{sp} and low thrust operation.

IV. Electromagnetic Thrust Vectoring in FPPT

4.1. Electromagnetic Thrust Vectoring Approach

Thrust vectoring/steering with the FPPT system has emerged as a highly desirable capability for the purposes of spacecraft attitude control and for desaturating attitude control reaction wheels, particularly for deep space missions where a spacecraft is beyond Earth's electromagnetic field so that magnetic torque rods or coils can no longer be used for wheel desaturation. Potential users of the FPPT technology have indicated that the vectoring/steering capability is of critical importance for certain missions (especially deep space), and as a result CUA has investigated electromagnetic vectoring by using embedded electromagnets behind the insulator positioned between the anode and cathode, **Figure 14**.

The FPPT produces thrust through the interaction of a pulse current of tens of kiloamperes with the azimuthal magnetic field self-generated by that current. FPPT thrust vectoring for control of pitch, yaw and roll, and the desaturation of reaction wheels, is achieved via a selective introduction of axial magnetic field (B_z) patterns to create $j_r B_z$ force components normal to the thruster axis [Woodruff, 2021]. Multi-coil vectoring uses applied magnetic fields from multiple auxiliary solenoid coils located in the FPPT insulator. Because the FPPT thrust is predominantly electromagnetic (EM), thrust vectoring is achieved by deflecting the *jxB* force vector off-axis to achieve pitch and yaw control, and by creating a swirl flow in the exhaust with a $(j_r B_z)_\theta$ force to provide roll control torque.

Quad-coil vectoring is implemented by imbedding four independently controlled and reversible B_z electromagnets, radially positioned between the anode and cathode and insulated from the discharge. The coil design is optimized to maximize the magnetic B_z field volume in the discharge region. These fields couple selectively with the radial thruster plasma discharge current to provide off-axis thrust in order to provide positive or negative pitch or yaw motion to the spacecraft, **Figure 14(left)**. If two opposite coils or all four coils are energized with matched polarity the $(j_r B_z)_\theta$ force imparts a rotational torque to the plasma flow to generate spacecraft roll, **Figure 14(right)**. Torque in the reverse direction is created by controlling the electromagnets to reverse the direction of the active coil B_z fields. The coil currents are supplied from a common supply, and each can be fed through an H-bridge MOSFET (**Figure 15**). The function of each H-bridge is to reverse the coil current when desired and therefore the applied Bz field.

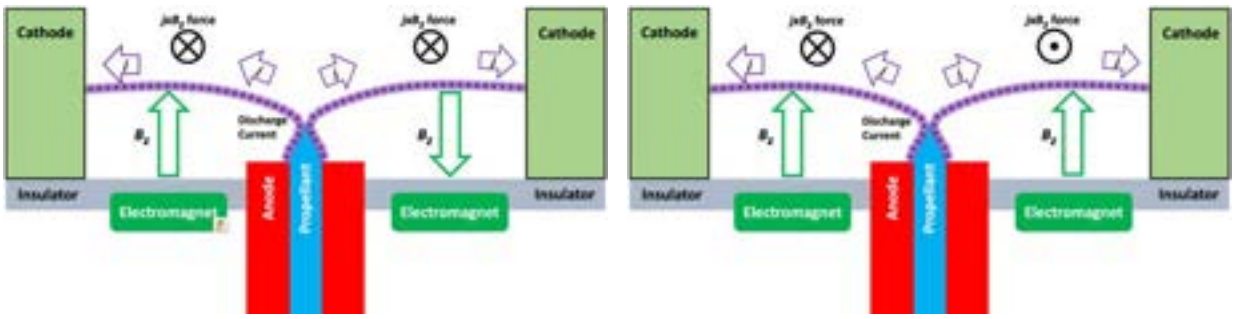

Figure 14. Electromagnetic Quad-Coil Vectoring approach using EM coils to: (left) induce pitch or yaw depending on the directions of current flow through the coils and the corresponding induced B-field; and (right) using 2 or 4 EM coils to induce roll by controlling the directions of the current flow through the coils and the corresponding induced B-field.

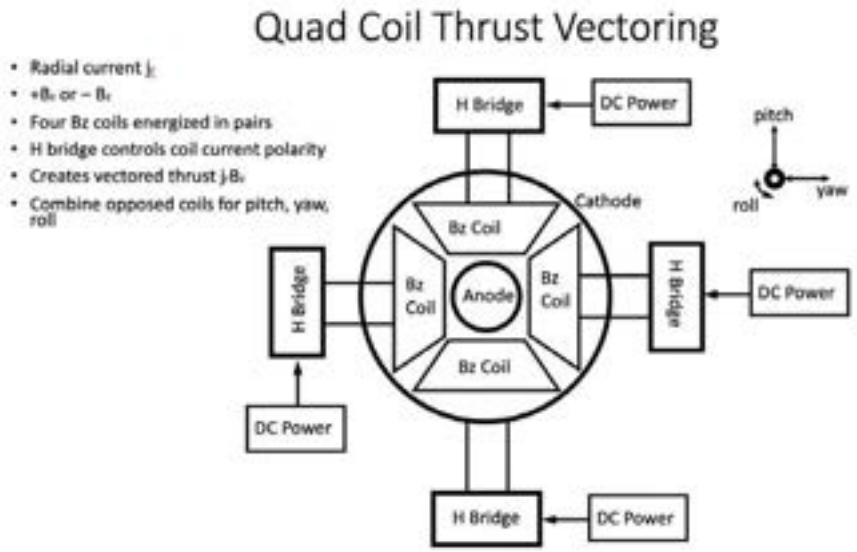

Figure 15. Quad coil thrust vectoring with applied Bz field from a four-coil system to create jrBz force components normal to the primary axial thrust vector.

The self-induced azimuthal (B_θ) magnetic field near the anode from a 20 kA FPPT primary discharge is on the order of 0.25 Tesla. With quad-coil vectoring, each EM coil is designed to produce a mean axial (B_z) magnetic field in the primary discharge region of 0.05 – 0.10 Tesla. Because the FPPT is a pulsed device with a pulse duration of tens of microseconds and a pulse repetition rate of several Hertz, the duty cycle when a coil may be energized is 10^{-4} – 10^{-5}, minimizing power consumption and coil heating.

The applied B_z field is perpendicular to the radial discharge current and provides a local azimuthal force $(\vec{j} \times \vec{B})_\theta$ on the accelerating thruster plasma in addition to the primary $j_r B_\theta$ force. Two such coils located 180 degrees apart but with opposed B_z fields then provide a net thrust perpendicular to the thruster axis. A total of four coils driven by positive or negative current provide both positive and negative pitch and yaw control. Two of the coils spaced 180 degrees apart, or all four coils having parallel matching +z or -z B_z fields provide an azimuthal torque to initiate positive or negative roll. Quad-coil vectoring requires 1 primary discharge circuit and 4 coil circuits.

4.2. Experimental Setup to Verify Thrust Vectoring

It is estimated that a 0.05 - 0.10 Tesla field strength is required to alter the B-field enough to vector thrust. Kovar rods for core material were chosen for preliminary testing, as they have high relative permeability (~2000 depending on heat treatment). Furthermore, it is likely that they will be imbedded in the thruster insulator for a final design, and Kovar has favorable thermal expansion properties. The coil parameters are shown in **Table 5**.

Table 5. Electromagnet sizing.

Electromagnet Parameters		
Core Material	Kovar	
Core Diameter	0.25	in
Core Length	1	in
Winding Gauge	26	AWG
Coil Turns	300	
Coil Resistance	1	Ohm
Coil Inductance	1.2	mH

A fully operational system would have 4 of these coils, although for simulated testing only 2 were used for yaw axis vectoring. As the thruster has radial symmetry, the additional axis is expected to function similarly if installed and tested. **Figure 14** shows the original diagram of the electromagnet locations and their assumed interactions on the thrust.

The modifications to a breadboard thruster, including electromagnets and mounting scheme are shown in **Figure 16**. A thinner insulator was used for this testing to decrease distance between the magnets and the main thruster discharge to mitigate the $1/x^3$ decay in the dipole electromagnetic field over distance. With 6 amps current, these magnets are capable of producing over 0.15 Tesla at their surface, decaying with distance. The magnets have Kovar cores, and a keyed socket was developed to position them as close as possible to the thrust chamber (see **Figure 16**). A slowly rising overdamped electromagnet current pulse with a pulse width of several hundred microseconds is supplied by the same switch circuit used to fire the igniters and is timed such that the peak current occurs at the same time as the thruster discharge.

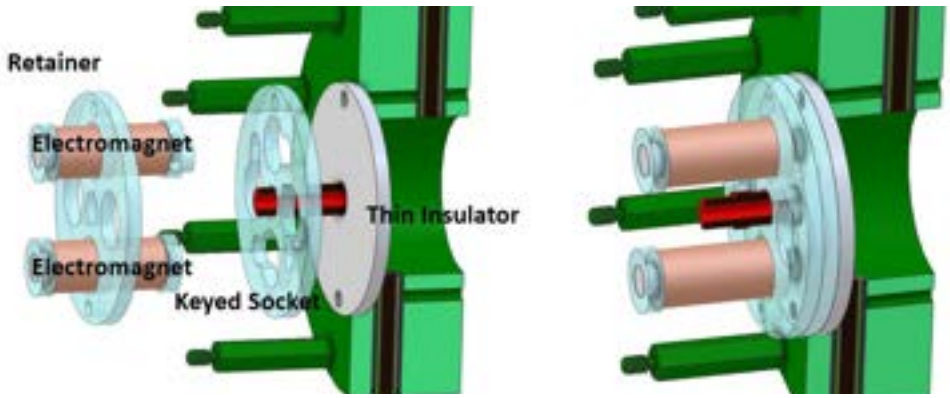

Figure 16. Exploded view (left) and assembled view (right) of EM thrust vectoring configuration with 2 coils.

With the electromagnets in a vertical plane as shown, thrust vectoring occurs in the horizontal plane and is measurable on the thrust stand. **Figure 17** shows the test hardware implemented, but disassembled, and **Figure 18** shows the back of the cathode with magnets installed, and a crossover, series connector in place. This allows a single supply to drive both coils in the directions favorable for yaw control. If the coils are connected to create parallel fields, roll would be produced, which cannot be measured on a conventional thrust stand.

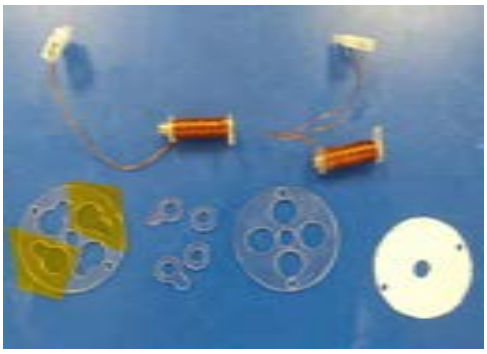

Figure 17. Components for EM quad coil thrust vectoring.

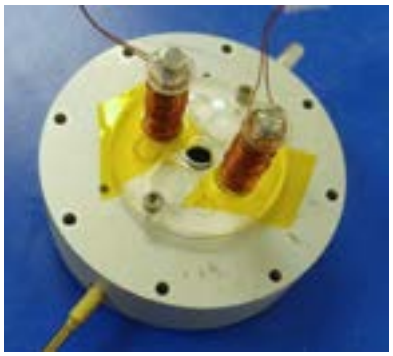

Figure 18. Assembled unit with electromagnets installed.

To ensure enough field strength to vector the thrust, as well as minimize heating of the magnets, a pulsed system was implemented using the high voltage switched igniter circuit. This allowed 10s of joules to be discharged through the coils, limited by a maximum voltage (1.2 kV). The pulse configuration is shown in **Table 6** and can be compared to the energy in the main thruster discharge, **Table 7**.

Table 6. Thrust vectoring current.

EM Vector Current Pulse		
Total Capacitance	89	µF
Voltage	300	V
Total Energy (2.0 J per coil)	4.0	J
Peak Current	76	A
Time to Peak Current	264	µs

Table 7. Primary thruster current.

Primary Thruster Current Pulse		
Total Capacitance	87	µF
Voltage	800	V
Total Energy	27.8	J
Peak Current	17.0	kA
Time to first reversal	10	µs

The coil current pulse is timed to the thruster current pulse. Fortunately, the thruster fires within a few microseconds of the igniter firing, but peak magnet current occurs approximately 260 microseconds after firing. Thus, the thruster firing is delayed by the same 260 microseconds in order to encounter maximum B-field.

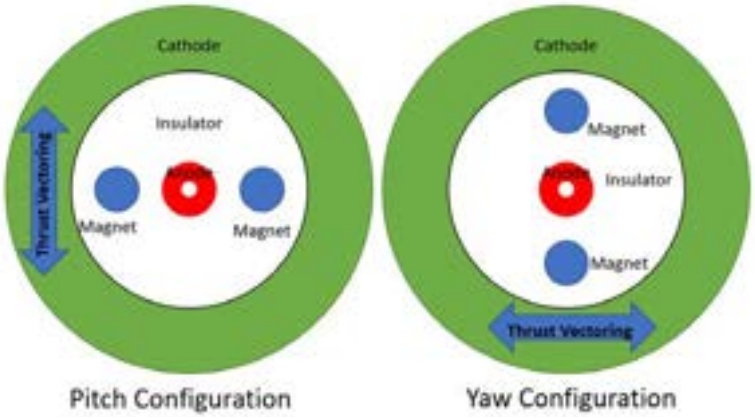

Figure 19. Orientation of two electromagnets and corresponding direction anticipated for thrust vectoring. Thrust stand motion is normal to the pitch vector and is parallel to the yaw vector.

4.3. Experimental Testing and Verification

Thrust vectoring was tested on the CUA thrust stand with a horizontally moving platform**. Figure 19** illustrates how the two electromagnets were positioned for the thrust stand measurements and the corresponding directions of pitch and yaw control. The thruster axis was aligned at 45 degrees to the thrust stand motion (**Figure 20**). With the thruster in the plus or minus pitch configuration the detected thrust with pitch vectoring is reduced by $\cos(\beta)$, where β is the angle of thrust deflection, inducing a small and similar effect for the two polarities. With the thruster in the plus or minus yaw configuration the thrust stand detects a thrust proportional to $cos(45 \pm \beta)$, an easily detectable variation on the thrust stand.

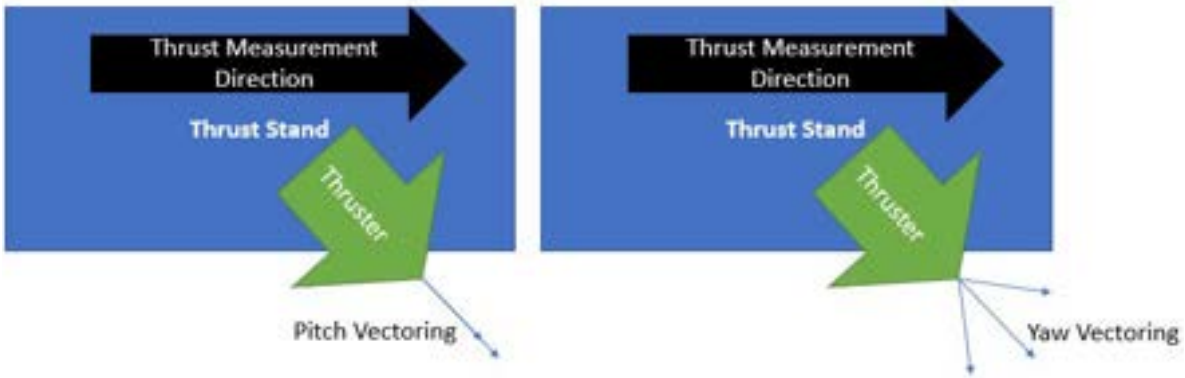

Figure 20. Thruster positioned at 45-degrees to the thrust stand motion. Pitch vectoring slightly decreases the thrust measurement. Yaw vectoring significantly increases or decreases the thrust measurement depending on magnet polarity.

Figures 21 and **22** show the measured thrust stand data of this system in operation for pitch and yaw. As expected, **Figure 21** shows small and approximately equal reductions in thrust when pitch is vectored up and down. When yaw is vectored, **Figure 22,** thrust was observed to be approximately constant in one direction, but drops significantly in the other direction. From this data, an estimated thrust deflection angle β can be calculated. The measurements are consistent if it is assumed that there is a ≈15% total loss of thrust with the electromagnets turned on, and that the *thrust vector angle is* $\beta \approx 10$ degrees. This gives cos(β) = 0.985, cos(45-β) = 0.82 and cos(45+β) = 0.57, accounting for the large polarity effect seen in **Figure 22**, and the small variations shown for the pitch test configuration in **Figure 21**. While more testing is planned at other mounting angles and at higher mean thrust rates in order to derive a more precise value for β, it is clear that the measured level of vectoring is sufficient to provide pitch and yaw control, and reaction wheel desaturation.

Roll torque, while not measured, can be estimated from the yaw measurements, and is estimated to be of the same order of magnitude when applied to reaction wheel desaturation.

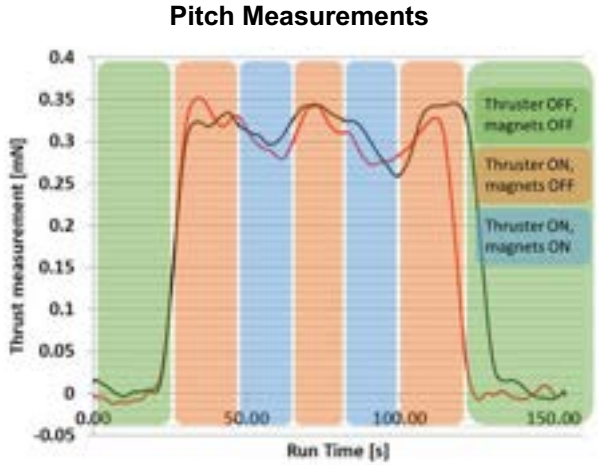

Figure 21. Raw thrust stand results for pitch measurements. Thruster is mounted at 45 degrees on thrust stand (Figure 13). Expected result would be equal, reduced thrust for both current directions when the magnets are enabled.

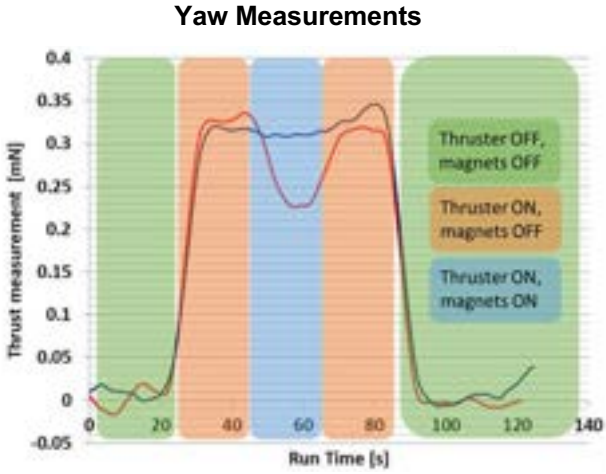

Figure 22. Raw thrust stand results for yaw measurements. Thruster is mounted at 45 degrees on thrust stand (Figure 13). Expected result would be a decrease in thrust in forward current direction (red) and an increase in thrust with reverse current direction (black).

These preliminary tests have demonstrated that there is sufficient field strength to deflect the thrust vector. Furthermore, reducing coil voltage from 300 to 200V still produced a strong effect, and the capacitor configuration needed to supply sufficient charge at this voltage using flight-like capacitors is of identical size to the small charge used in the igniter circuits. Refinement of the electromagnets by increasing the mean B_z in the interelectrode volume can fine tune the FPPT to provide vectoring of ± 10° with fewer losses, and potentially with lower current pulse energy.

In order to verify that the previously measured vectoring was not deflecting plasma into the cathode walls, the test setup was modified to use a shorter cathode, thereby reducing cathode wall interference with the thrust vector. Furthermore, a thicker, standard insulator was used, which reduces B_z. The thruster was placed on the thrust stand at an approximate 45° angle as measured clockwise from the thrust stand's measurement axis. These tests were also run at a higher pulse rate of 4 Hz to reduce error. As seen in **Table 8,** an increase in thrust was detected when the electromagnets were turned on with current flow in the "reverse" direction, and a decrease in thrust was detected with current flow in the "forward" direction. In this test, the electromagnets are placed in the yaw configuration because this produces the most easily detectable change in thrust direction on the thrust stand.

From the thrust data at 0° the actual angle of the thruster assembly during this test was calculated to be approximately 41° (rather than 45°). *The thrust data presented in **Table 8** is consistent with a thrust vectoring angle of 9.2° and a two-percent decrease in overall thrust.* The effect is also captured in photographs shown in **Figures 23 and 24**, where an asymmetrical thruster plume is visible. **Figures 25 and 26** are photographs that show the concentration of cathode spots (indicating current attachment) on the same side of the thruster as the asymmetrical plumes.

Table 8. Short cathode vectoring thrust results (yaw configuration).

Electromagnet State	Orientation	Average Ibit [μN-s]
Off	0°	132
Off	41°	100
"Forward"	41°	83
"Reverse"	41°	110

Figure 23. Thruster firing with electromagnets turned on with current flow in the "forward" direction. Camera is looking down from above.

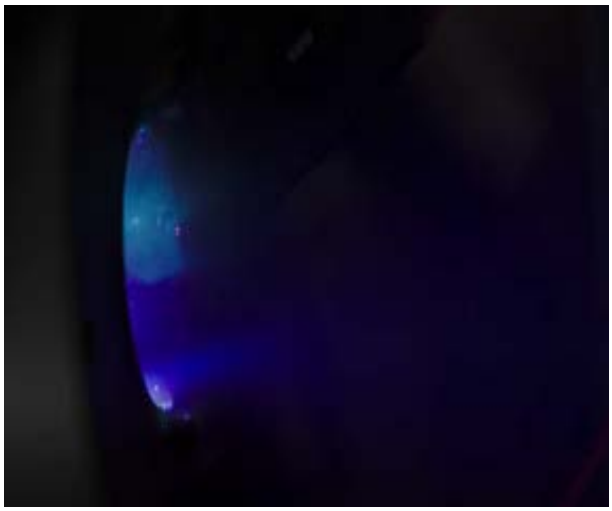

Figure 24. Thruster firing with electromagnets turned on with current flow in the "reverse" direction. Camera is looking down from above.

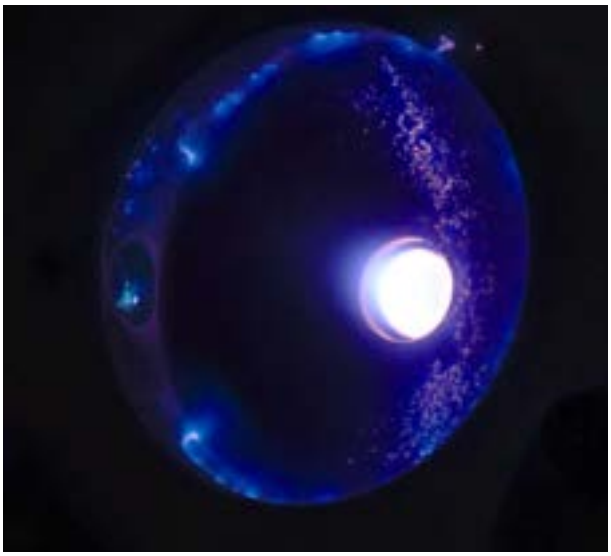

Figure 25. Thruster firing with electromagnets turned on with current flow in the "forward" direction.

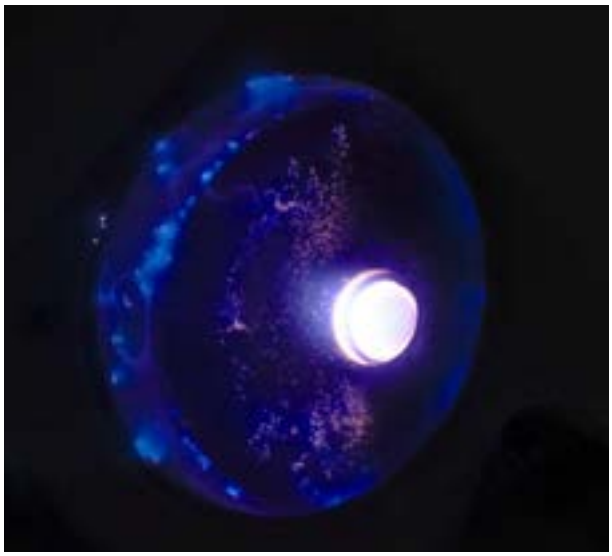

Figure 26. Thruster firing with electromagnets turned on with current flow in the "reverse" direction.

4.4. Reaction Wheel Desaturation

The FPPT with multi-coil thrust vectoring can be used to desaturate onboard reaction wheels (1, 2, or 3-axis) for spacecraft. An ancillary design requirement is that the spacecraft center of gravity (CG) lies close to the FPPT geometric axis, and a distance of a couple of millimeters is suggested, as may be achieved with off-axis balance masses. As a corollary, the CG of the propellant spool must also lie on the FPPT axis and remain there as propellant is consumed.

For pitch and yaw calculation purposes, it is assumed that the thrust axis is vectored such that the torque lever arm d at the CG is = 5 mm, corresponding roughly to a vector deflection angle of 5 degrees. For a given thruster impulse bit Ibit, the torque impulse bit is then $T_{bit} = d*I_{bit}$. From existing FPPT thrust stand data the thrust for a 32 J bank at 1.3 Hz is 0.35 mN, leading to a 16 J I_{bit} of 0.125 mN-s and T_{bit} = 0.625 μN-m-s/pulse.

For example, for a CubeSat magnetic gyroscope with a saturated angular momentum of L = 0.011 N-m-s, the number of pulses needed is then 17,600. At a pulse rate of 2 Hz, this will take 2.5 hours to desaturate 1 wheel and 5 hours to desaturate both pitch and yaw. It is expected that similar times will be characteristic of roll control and roll wheel desaturation.

V. Design and Fabrication of Flight FPPT System for DUPLEX CubeSat

CUA was selected for a NASA STMD Tipping Point award to fabricate and fly the 6U "Dual Propulsion Experiment (DUPLEX)" CubeSat with one FPPT flight unit and another CUA thruster technology, the Monofilament Vaporization Propulsion (MVP) system [Woodruff, 2018; Woodruff, 2022]. The DUPLEX mission is manifested for launch in Q1 2023 to be deployed from the Northrop-Grumman NG-19 Cygnus resupply vehicle, followed by in-space operations with the FPPT and MVP thrusters. This mission will provide flight heritage, take both technologies to TRL 8-9, and encourage customer acceptance of these new propulsion systems.

Dimensioned drawings of the FPPT flight unit exterior are shown in **Figure 27** and the 1.7U FPPT flight unit design is illustrated in **Figure 28**. This design features a 4-module 32 J ESU and >800 g PTFE fiber along with the feed motor, storage spool, multiple igniters, and ESU charging / motor controller / discharge ignition circuits. The estimated performance of the 1.7U FPPT system is listed in **Table 9**. The FPPT flight-like and flight units will undergo an extensive series of planned testing including environmental (vibe, TVAC, EMI), thrust stand burn in and performance testing, center of gravity, moment of inertia, and operational modes analyses.

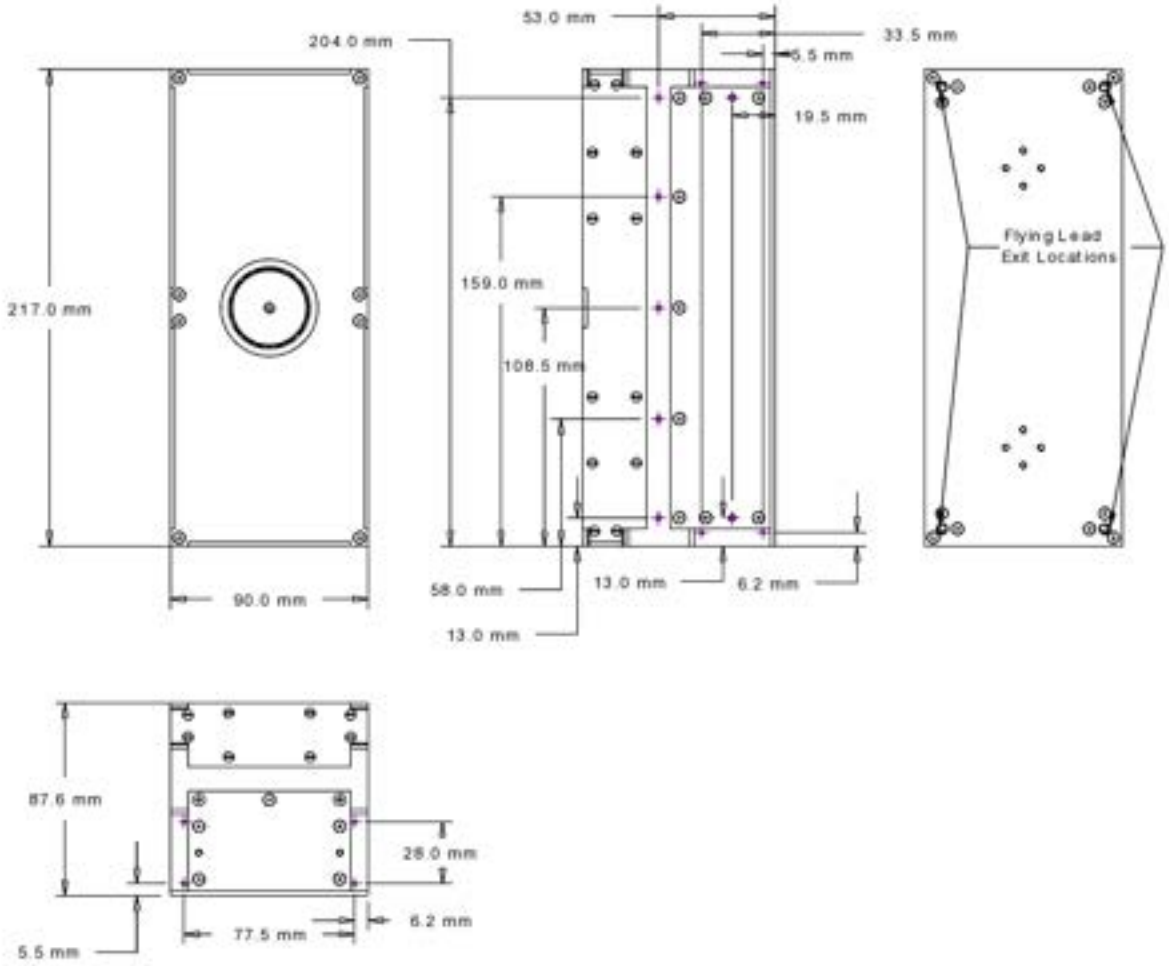

Figure 27. Dimensioned drawings of external housing of the FPPT flight system for the DUPLEX 6U CubeSat mission.

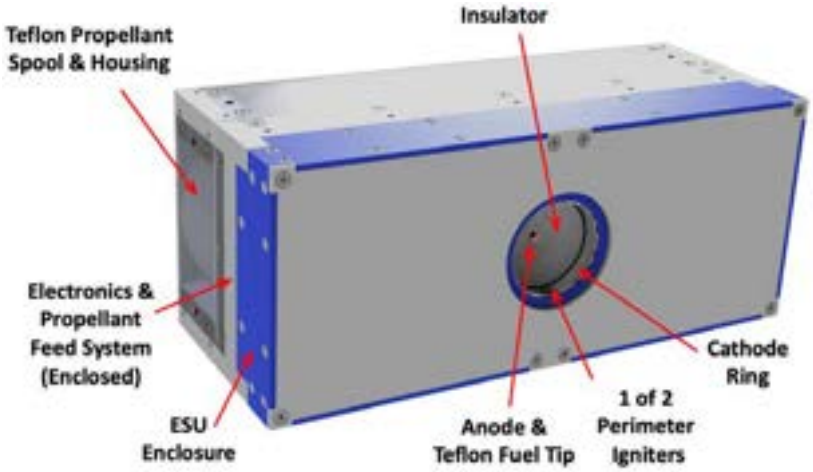

Figure 28. Image of 1.7U FPPT flight unit highlighting primary components and structural elements.

Table 9: System performance of a 1.7U FPPT: estimated performance of flight FPPT system for DUPLEX 6U CubeSat based upon subsystem performance testing. [Note: the duty cycle is still to be determined with flight unit testing.]

Item	Estimated "Flight" FPPT Performance
Propulsion system dimensions	9.0 x 8.76 x 21.7 cm^3
Propulsion system volume	1,711 cm^3
Survival temperature range	– 35°C to + 80°C
Propellant	PTFE (Teflon), 2.2 g/cc storage density
Power to FPPT system when firing	48 W (1.5 Hz)
Capacitor Bank Energy	32 J
PPU efficiency	~0.75 (3 Hz, improves at lower rates)
Duty Cycle	TBD (est. 1 Hz continuous operation)
Propellant Mass	827 g
Dry Mass	1,975 g
Total propulsion wet mass	2,802 g
Nominal mass flow rate	0.010 mg/s
Total thrust time	2.6 years
Specific Impulse	3,500 s
Thrust @ 48 W	0.33 mN
Thrust/Power	7 μN/W
Thrust Vectoring	Est. ±10° pitch and yaw (roll capability TBD)
Total impulse	28,000 N-s
Volumetric total impulse	16,600 N-s/liter
Spacecraft ΔV, M(initial) = 10.5 kg	2,820 m/s

VII. Concluding Remarks

CUA has successfully developed the FPPT from concept to 1.7U flight design. During development testing, over 1 million pulses have been executed on the breadboard FPPT system, and over 1.6 billion pulses have been executed on a subscale life-test ESU. A regenerative carbon igniter was fabricated and used successfully for discharge initiation. Due to its regenerative nature, igniter erosion has not been found to be life-limiting [Woodruff, 2019]. An accelerated test on the FPPT igniter circuit was run and demonstrated >150 million pulses without failure. The FPPT performance envelope can be broadened by varying the fuel feed rate. Fuel feed can be adjusted to vary specific impulse. Additionally, FPPT thrust is inherently 0 – 100% throttleable by varying pulse rate. Testing to date shows electromagnetic thrust vectoring capabilities on the order of ±10 degrees in the pitch and yaw axes. Furthermore, the system has the potential to provide control authority on the roll axis. The pitch and yaw thrust vectoring performance are presented alongside recent thruster performance improvements.

A 1.7U FPPT with 28,000 N-s of total impulse is being fabricated and assembled for flight integration in CUA's NASA-funded Dual Propulsion Experiment (DUPLEX) CubeSat, presently manifested for launch in Q1 2023. This 1.7U FPPT system configuration has a 26 J energy storage unit (ESU) that can operate at 78 Watts (3 Hz) producing a mean thrust of 0.60 mN with a specific impulse of 3,500 s and an efficiency of 13%. The system will also include thrust vectoring electronics. This mission will provide flight heritage for FPPT, increase the system TRL to 8-9, and encourage customer acceptance of this new propulsion system.

CUA sees FPPT technology as a compelling option to meet many micropropulsion needs including collision avoidance maneuvers, extended orbit raising/lowering maneuvers, inclination change, drag makeup, and deorbiting. Further, thrust vectoring/steering with the FPPT system has emerged as a highly desirable capability for the purposes of spacecraft attitude control and for desaturating attitude control reaction wheels, particularly for deep space missions where a spacecraft is beyond Earth's electromagnetic field so that magnetic torque rods or coils can no longer be used for wheel desaturation. FPPT thrusters are expected to provide a compact, lightweight, non-hazardous propulsion technology solution, available in a family of sizes. FPPT requires no safety equipment for storage, transportation, integration, and testing, and places no demanding requirements on the launch provider, making it an attractive low-cost solution for NASA, DOD, industry, research, and academic CubeSat and small-satellite missions.

VIII. Acknowledgments

This work was supported by NASA's SBIR program on contract numbers NNX17CP36P and 80NSSC18C0063 (technical monitor Richard Hofer of the NASA Jet Propulsion Laboratory), by NASA's Space Technology Mission Directorate on contract # 80ARC020C0001 (technical monitor Ali Guarneros Luna at Ames Research Center) for the DUPLEX CubeSat program, and by CUA Internal Research and Development funds. Our thanks to Eric Pencil and Louis Pinero of NASA Glenn Research Center for invaluable discussions regarding the electronics and proper grounding of space rated PPT systems. We also thank Iain Murphy and Mark Smart for assistance with the build, inspection, and subsystem testing of the packaged FPPT system.

IX. References

Benson, S. W., Arrington, L. A., Hoskins, W. A. and Meckel, N. J., "Development of a PPT for the EO-1 Spacecraft," NASA TM-2000-210340, AIAA Paper # 99-2276, 2000.

Burton, R. L., K.E. Clark, K. E., and Jahn, R. G., "Measured performance of a multimegawatt MPD thruster," *Journal of Spacecraft and Rockets*, Vol. 20, No. 3, 299–304, 1983.

Burton, R. L. and Turchi, P. J., "Pulsed Plasma Thruster," *J. Propulsion and Power*, Vol. 14, No. 5, 716, 1998.

Burton R L, Woodruff C A, King D M, and Carroll D L, "Analysis of Fiber-fed Pulsed Plasma Thruster Performance," *J. of Propulsion and Power*, Vol. 37, No. 1, pp. 176-178, 2021.

Ekdahl, C., Kribel, R., and Lovberg, R., "Internal Measurements of Plasma Rotation in an MPD Arc," AIAA Paper # 67-655, 1967.

Ebert, W. L., Kowal, S. J., and Sloan, R. F., "Operational Nova Spacecraft Teflon Pulsed Plasma Thruster System," AIAA Paper # 89-2497, 1989.

Guman, W. J., "Switch-Triggered Pulse Plasma Accelerator Thrust Measurements," AIAA J., **3** (6), 1158, 1965.

Guman W. J. and Nathanson, D. M., "Pulsed Plasma Micro-thruster Propulsion System for Synchronous Orbit Satellite," *J. Spacecraft and Rockets*, **7** (4), 409-15, 1970.

Hejmanowski, N. J., Woodruff, C., Burton, R.L., Carroll, D.L., and Cardin, J., "CubeSat High Impulse Propulsion System (CHIPS)," *62nd JANNAF Propulsion Meeting (7th Spacecraft Propulsion)*, Paper Tracking # 4032 (2015).

Hoffman, E. J., "Spacecraft Design Innovations in the APL Space Department," Johns Hopkins APL Technical Digest, Vol. 13, No. 1, 167-181, 1992.

Jahn, R. G., "Physics of Electric Propulsion." McGraw-Hill, New York, 1968.

Laystrom, J., Burton, R., and Benavides, G., "Geometric Optimization of a Coaxial Pulsed Plasma Thruster", AIAA Paper # 2003-5025, 2003.

Lemmer, K, "Propulsion for CubeSats," *Acta Astronautica*, 134, 231 (2017).

Woodruff C., Carroll D., King D., Burton R., and Hejmanowski N., "Monofilament Vaporization Propulsion (MVP) – CubeSat propulsion system with inert polymer propellant," *Small Satellite Conference*, Logan, UT, Paper # SSC18-III-09 (2018).

Woodruff, C., King, D., Burton, R., Bowman, J., and Carroll, D., "Development of a Fiber-Fed Pulsed Plasma Thruster for Small Satellites," Small Satellite Conference, Paper # SSC19-WKVIII-06, 2019a.

Woodruff, C., King, D., Burton, R., and D. Carroll, "Fiber-fed Pulsed Plasma Thruster for Small Satellites," *36th International Electric Propulsion Conference (IEPC) 2019*, Vienna, Austria, Paper # IEPC 2019-899, 2019b.

Woodruff, C., King, D., Burton, R., Carroll, D., and Parta, M., "Fiber-Fed Advanced Pulsed Plasma Thruster (FPPT) – Continuation-in-Part", U.S. Patent Application 17/559,178, 2021.

Woodruff, C., Parta, M., King, D., Woodruff, A., Burton, R., and Carroll, D., "Monofilament Vaporization Propulsion Systems," *37th International Electric Propulsion Conf.*, Cambridge, MA, Paper # IEPC 2022-575, 2022.

Zakrzwski, C., Benson, S., Sanneman, P., and Hoskins, A., "On-Orbit Testing of the EO-1 Pulsed Plasma Thruster, " AIAA Paper # 2002-3973, 2002.